NASA TECHNICAL NOTE

NASA TN D-2057

C. 1

LOAN COPY:
AFWL (
KIRTLAND /

TECH LIBRARY KAFB, NM
0154631

NASA TN D-2057

STATIC LONGITUDINAL CHARACTERISTICS OF THE PROJECT FIRE REENTRY STAGE AFTER REENTRY-PACKAGE SEPARATION AT MACH 28.3 IN HELIUM

by Curtis D. Snyder

Langley Research Center
Langley Station, Hampton, Va.

NATIONAL AERONAUTICS AND SPACE ADMINISTRATION • WASHINGTON, D. C. • JANUARY 1964

TECH LIBRARY KAFB, NM

0154631

STATIC LONGITUDINAL CHARACTERISTICS OF THE PROJECT FIRE REENTRY STAGE AFTER REENTRY-PACKAGE SEPARATION AT MACH 28.3 IN HELIUM

By Curtis D. Snyder

Langley Research Center
Langley Station, Hampton, Va.

NATIONAL AERONAUTICS AND SPACE ADMINISTRATION

For sale by the Office of Technical Services, Department of Commerce,
Washington, D.C. 20230 -- Price $0.50

STATIC LONGITUDINAL CHARACTERISTICS OF THE PROJECT FIRE REENTRY STAGE AFTER REENTRY-PACKAGE SEPARATION AT MACH 28.3 IN HELIUM

By Curtis D. Snyder

SUMMARY

An experimental force and moment investigation has been conducted on a 0.05-scale model of the rocket motor case with adapters attached which will accelerate an instrumented spacecraft to 37,000 feet per second during a future flight-reentry program. The purpose of this investigation was to obtain data which would aid in determining whether the rocket motor would maintain adequate separation from the reentry package during reentry. The tests were conducted in helium at a Mach number of 28.3 and a Reynolds number of 0.68×10^6 based on rocket-motor diameter. Data were obtained over an angle-of-attack range from 0° to 180°.

High-speed schlieren photography was employed in an investigation of anomalies in the data at specific angles of attack. Discontinuities in the drag and pitching moment are shown to be caused by nearly instantaneous changes in the shock-wave pattern as the attitude of the model was varied.

INTRODUCTION

Project Fire is a Langley Research Center project formulated to further information concerning flight reentry sciences associated with entry into the earth's atmosphere at hyperbolic velocities. Ballistic flight tests of rocket-boosted instrumented spacecraft are planned to determine total heat transfer, ultra-high-temperature air radiance, materials response, and radio-blackout effects. The Project Fire vehicle consists of a reentry package which is attached by an adapter to an Antares II (X-259) rocket motor. These components are enclosed by a shroud and a guidance-unit shell. This assembly (designated velocity package) will be launched on a ballistic trajectory by an Atlas D first-stage launch vehicle. Prior to entering the atmosphere, the Antares motor will accelerate the reentry package to a velocity of about 37,000 feet per second. After rocket-motor burnout, the reentry package will separate from the Antares motor and enter the atmosphere. After the initial separation of the reentry package from the rocket motor, both configurations will be outside the sensible atmosphere and will thus be following essentially a ballistic trajectory. Since both configurations will enter the atmosphere only slightly separated and on the same flight path, some action must be initiated to ensure the separation necessary to avoid collision and to facilitate tracking.

In order to assess the seriousness of the separation problem, it was first necessary to investigate the aerodynamic characteristics of the rocket-motor case with the adapters attached (i.e., the Project Fire reentry stage after reentry-package separation).

The tests for determining the forces and moments on a 0.05-scale model of this configuration over an angle-of-attack range from 0° to 180° were made in the Langley 22-inch helium tunnel in support of the overall project. The configuration, shown as the shaded portion of figure 1, consists of the Antares II (X-259) rocket motor with the reentry package adapter and the Antares adapter ring attached. The test program was conducted in helium at a Mach number of 28.3 and a Reynolds number of 0.68×10^{6} based on rocket-motor diameter. The results of the present test program are presented herein.

SYMBOLS

A drawing showing positive directions of forces and moments is presented in figure 2.

C_A	axial-force coefficient, $\frac{\text{Total axial force}}{qS}$
C_D	drag coefficient, $C_A \cos \alpha + C_N \sin \alpha$
C_L	lift coefficient, $C_N \cos \alpha - C_A \sin \alpha$
C_m	pitching-moment coefficient, $\frac{\text{Pitching moment}}{qSD}$
C_N	normal-force coefficient, $\frac{\text{Normal force}}{qS}$
D	diameter of rocket-motor case, 1.500 in.
M	free-stream Mach number
P_t	stagnation pressure, lb/sq in.
q	free-stream dynamic pressure, lb/sq in.
R	Reynolds number based on rocket-motor diameter
S	rocket-motor case cross-sectional area, 1.767 sq in.
α	angle of attack, deg

APPARATUS AND TESTS

The test program was performed in the Langley 22-inch helium tunnel which is shown in figure 3 and described in reference 1. The 5° half-angle conical nozzle used employed a 0.548-inch-diameter interchangeable throat. This nozzle-throat combination gives an area ratio sufficient to obtain Mach numbers near 30 in the test regions. The results of a survey performed to determine the Mach number distribution in the test region are shown in figure 4. The values of Mach number were calculated from total-pressure ratios obtained in the horizontal and vertical positions indicated by using the computation procedure described in reference 2 in conjunction with reference 3. The estimated accuracy of the Mach number is ±0.7 percent. Mach number distributions were determined at three longitudinal positions in the test region and indicated flow characteristic of that generated by conical nozzles in that both longitudinal gradients (the gradient for Mach number was 0.09 per inch) and flow divergence existed.

A flow-angularity survey was conducted to determine the degree of divergence present in the test section. The results of this investigation revealed that the maximum inclination of the flow within the high-speed core occupied by the model was less than 1.2°.

All tests were conducted at a stagnation pressure automatically regulated at 2,000 psig. The total temperature in the settling chamber remained essentially constant at 515° R for the duration of the tests. The Mach number at the nose of the model was 28.3 when the model was alined with the flow.

Forces and moments were measured with a sting-mounted strain-gage balance while the model was rotated in the pitch plane. The strain-gage-balance outputs were recorded automatically at predetermined attitudes by the data-acquisition system described in reference 1. The angle-of-attack range covered during each test was 36.5° at a rate of about 3° per second. The model was rotated through this 36.5° angle-of-attack range twice during each test (once in each direction) in order to obtain substantiating data. Therefore two data points are available for all values of angle of attack. Both values are plotted and the scatter thus shown can be taken as indicative of the overall accuracy associated with the procedure used in this test program.

A slight temperature effect existed during the last 15 seconds of the 25-second tests. This temperature effect was confined to the axial-force outputs and was accounted for in the data-reduction procedure. Base pressures were not measured since the model was continually rotated in pitch; the effect of base pressure is not expected to be large.

MODEL

Details of the 0.05-scale model are given in figure 5; the model represents the Project Fire reentry stage after reentry-package separation. In order to obtain data over the angle-of-attack range from 0° to 180°, it was necessary to construct three models, all identical except for the manner in which they were

supported by the sting. The alterations necessary to mount the model for a specified angle-of-attack range are shown in figure 6. Axial-force measurement at angles of attack near 70° was affected by the relocation of the balance sting assembly as is discussed subsequently in more detail. All models were constructed of aluminum and the exterior surfaces were polished.

RESULTS AND DISCUSSION

The basic results obtained from this investigation are presented in figures 7 to 9, and the longitudinal-performance data are shown in figures 10 and 11. Discontinuities are evident in the data at angles of attack near 133° and/or 148°. The anomalies prompted a photographic investigation, the results of which are discussed subsequently.

Force and Moment Investigation

The variation of axial-force coefficient and normal-force coefficient with angle of attack is shown in figures 7 and 8, respectively. Except for the irregularities in the data at $\alpha = 133^{\circ}$ and $\alpha = 148^{\circ}$, these figures display typical variations in C_N and C_A. The presence of the balance-sting assembly did affect axial force for angles of attack near 70°. As shown in figure 6, the balance-sting assembly was located through the nozzle of the rocket-motor model for $\alpha \leqq 70^{\circ}$; however, for the angle-of-attack range of $70^{\circ} \leqq \alpha \leqq 110^{\circ}$, the balance-sting assembly was mounted perpendicular to the model axis of symmetry. The disagreement in C_A near $\alpha = 70^{\circ}$ is attributed to the difference in the model-balance geometry, and it is believed that the axial-force data for $70^{\circ} \leqq \alpha \leqq 110^{\circ}$ are more correct than those for $50^{\circ} \leqq \alpha \leqq 70^{\circ}$ because from purely geometrical considerations, the perpendicular balance arrangement is more favorable.

The effects of angle of attack on pitching moment for the rocket-motor model are presented as the upper curve in figure 9. For the moment-reference center chosen (which is the anticipated center of gravity for the spent rocket motor with adapters attached), the experimental results indicate four trim points over the angle-of-attack range from 0° to 180°. Two of these trim points were stable; the stability at $\alpha = 16^{\circ}$ was limited to a small variation in angle of attack.

The lower curve of figure 9 is presented to attempt to explain the erratic behavior of C_m indicated in the upper curve. The rocket motor was tested without the reentry-package adapter or the Antares adapter for comparable values of angle of attack. Both configurations had identical moment-reference centers when measured from the rear of the nozzle. Comparison of the pitching-moment results for the two configurations reveals that the nonlinear trends evident in the upper curve of figure 9 are a result of the addition of the adapters; the detrimental effect on stability caused by the addition of such unconventional shapes is apparent.

The variation of lift coefficient and drag coefficient with angle of attack is presented in figures 10 and 11, respectively. The lift results indicate an

approximately zero initial lift-curve slope with maximum lifting force developed near an angle of attack of 57°. The drag results are similar to the normal-force results with maximum drag occurring near $\alpha = 85^{\circ}$.

Photographic Investigation

The extremely nonlinear trends at values of angle of attack near 133° and 148° aroused considerable speculation concerning the validity of the data and the nature of the responsible flow phenomena. In addition to the data that were sampled and plotted at discrete angles of attack, a continuous record of the balance outputs was made during each test. For those tests where the model was rotated through the attitudes in question (i.e., $\alpha = 133^{\circ}$ and 148°), the abrupt shifts were observed on this record and are reflected in the fairing of the data.

An investigation of the flow phenomena responsible for these discontinuities was made by using high-speed schlieren motion pictures of the shock-wave patterns. The results of the investigation corroborated the previous data in that instantaneous changes in shock-wave pattern were noted at the same angle of attack where the data exhibited abrupt shifts. These changes are shown in figure 12 where consecutive frames are displayed. A sketch (fig. 13) is presented to clarify the shock-wave pattern. The time interval between frames is about 1/3000 second.

As the angle of attack of the model was increased near $\alpha = 133^{\circ}$, pulsations developed in the shock patterns as a result of the hollow nozzle on the rocket-motor model. The frequency of the pulsation remained constant, but the amplitude (shock detachment distance) increased until an angle of attack of about 148° was reached. The shock-wave pattern then collapsed abruptly and the oscillations ceased.

CONCLUDING REMARKS

The static longitudinal-stability characteristics of a 0.05-scale model of the Project Fire reentry stage after separation from reentry package have been experimentally determined over the angle-of-attack range from 0° to 180°. The investigation was conducted in helium at a Mach number of 28.3 and a Reynolds number of 0.68×10^{6} based on rocket-motor diameter.

The data presented in this report were obtained in order that it might be employed in a computer study of the separation characteristics of the reentry package and the spent rocket-motor case. Preliminary results from this computer study indicate that the longitudinal and cross-range displacements are influenced by a number of factors and that the minimum acceptable separation distances might be difficult to ensure, collision being a possibility in some cases. Based on the results of the separation study, the system has been redesigned to maintain adequate separation.

A supplement to the present investigation using high-speed schlieren motion pictures of abrupt discontinuities at angles of attack of 133° and 148° was made to define the responsible flow phenomena. The anomalies in the forces and/or moments at these specific angles of attack are shown to be caused by instantaneous changes in the shock-wave patterns as the attitude of the model was varied.

Langley Research Center,
National Aeronautics and Space Administration,
Langley Station, Hampton, Va., October 10, 1963.

REFERENCES

1. Johnston, Patrick J., and Snyder, Curtis D.: Static Longitudinal Stability and Performance of Several Ballistic Spacecraft Configurations in Helium at a Mach Number of 24.5. NASA TN D-1379, 1962.

2. Erickson, Wayne D.: Real-Gas Correction Factors for Hypersonic Flow Parameters in Helium. NASA TN D-462, 1960.

3. Mueller, James N.: Equations, Tables, and Figures for Use in the Analysis of Helium Flow at Supersonic and Hypersonic Speeds. NACA TN 4063, 1957.

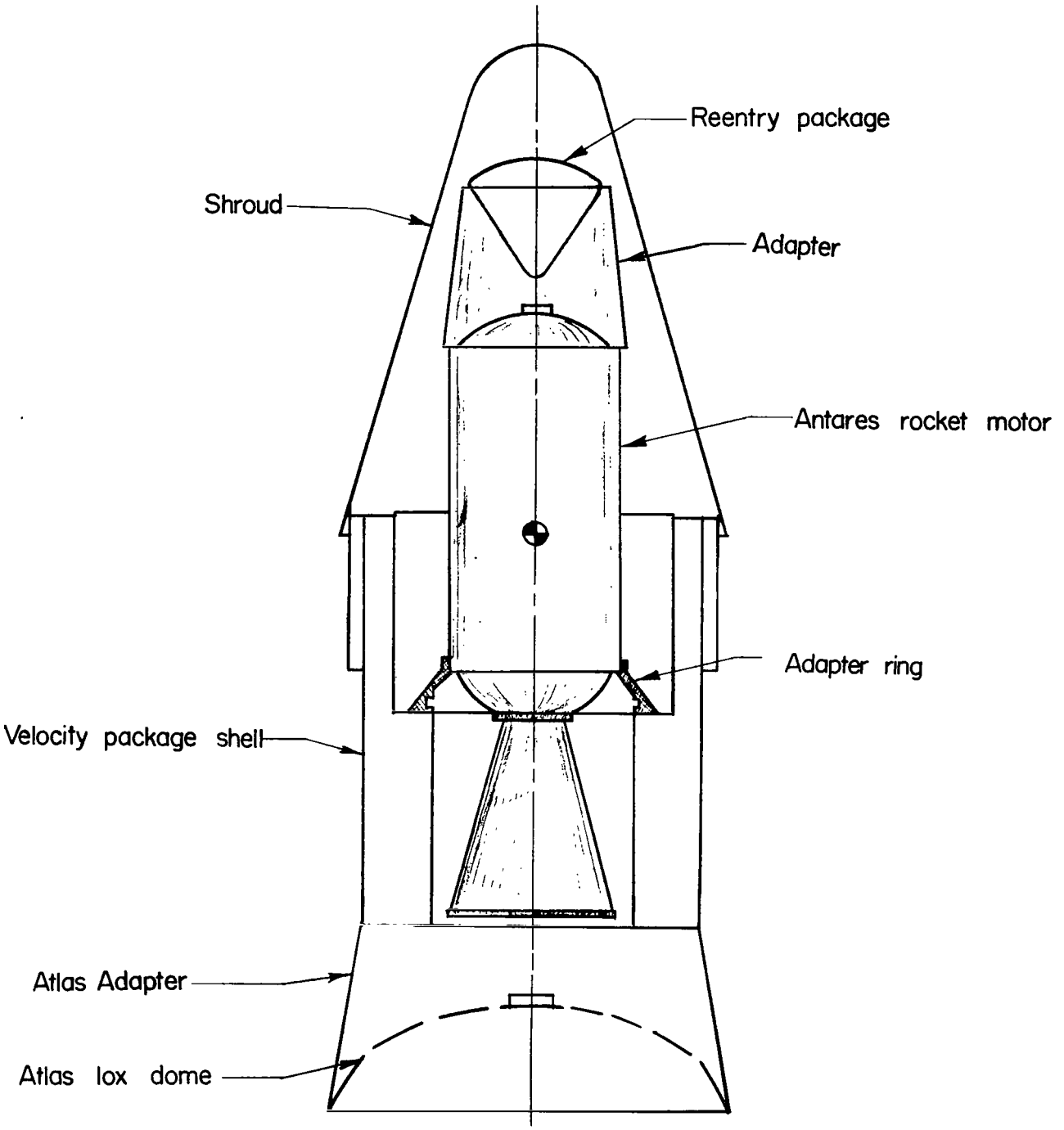

Figure 1.- Project Fire velocity package and Atlas adapter.

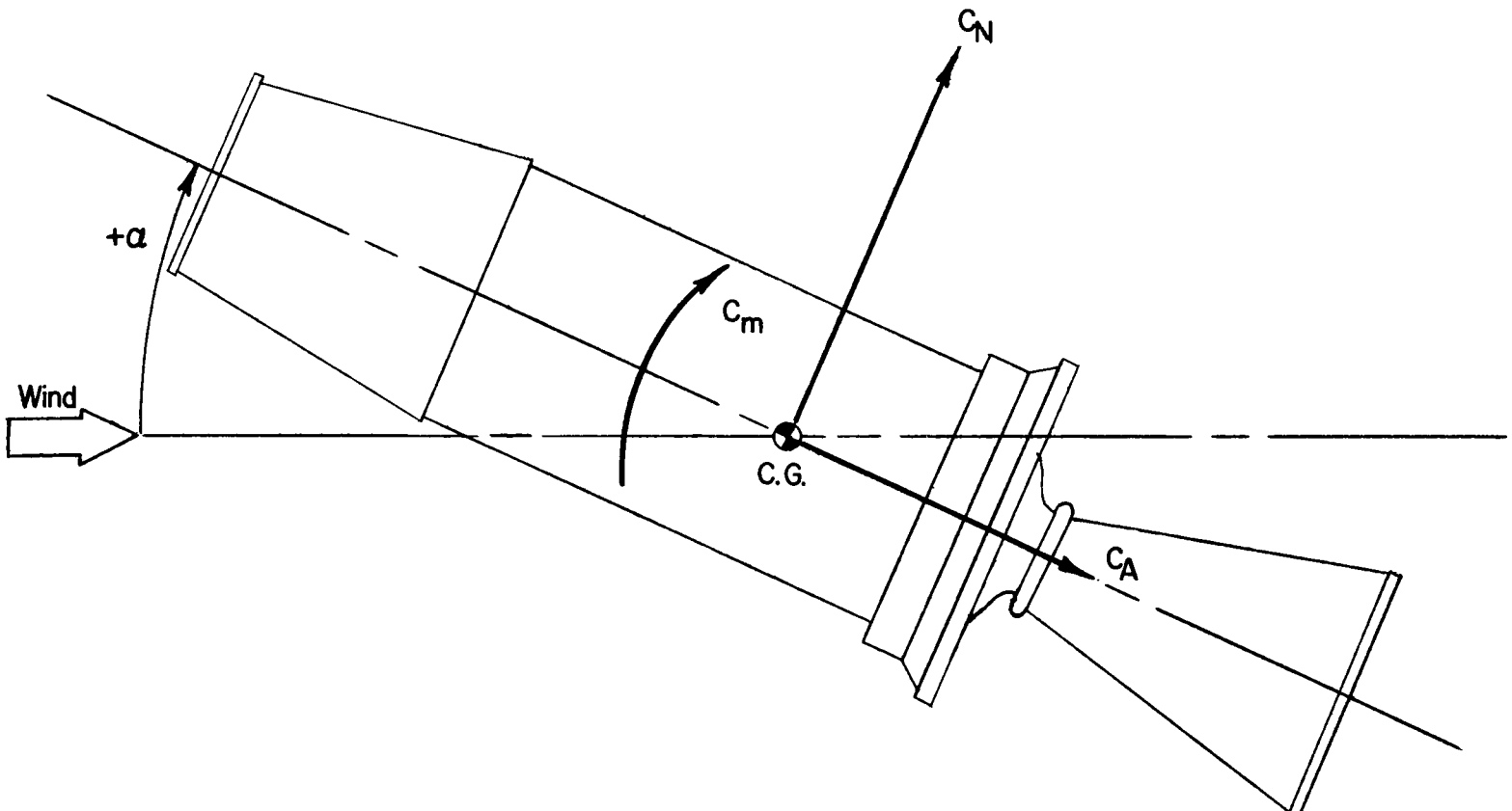

Figure 2.- Body-axis system. Positive directions indicated.

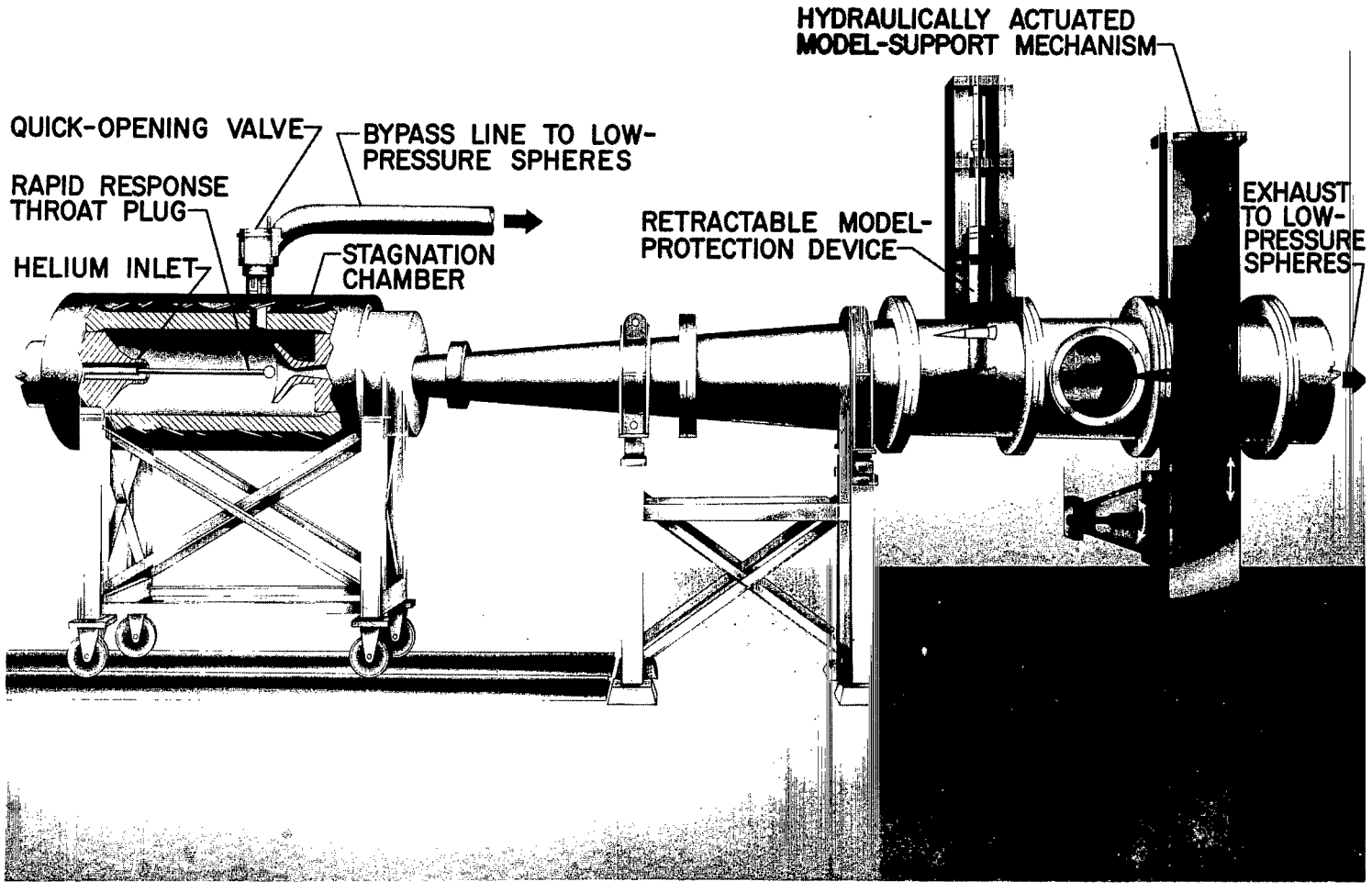

Figure 3.- Langley 22-inch helium tunnel.

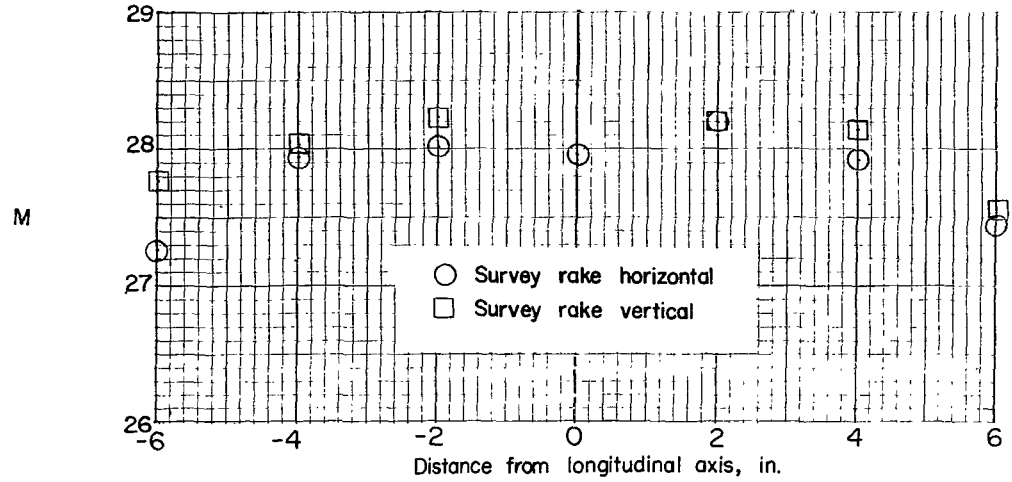

(a) 156.87 inches from throat.

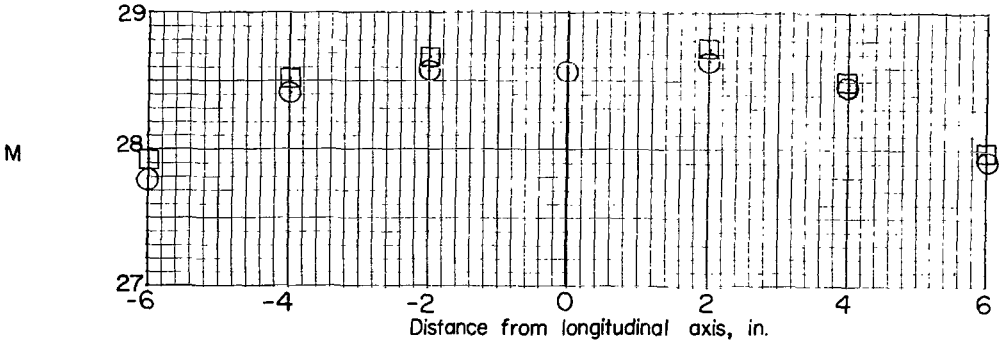

(b) 161.87 inches from throat.

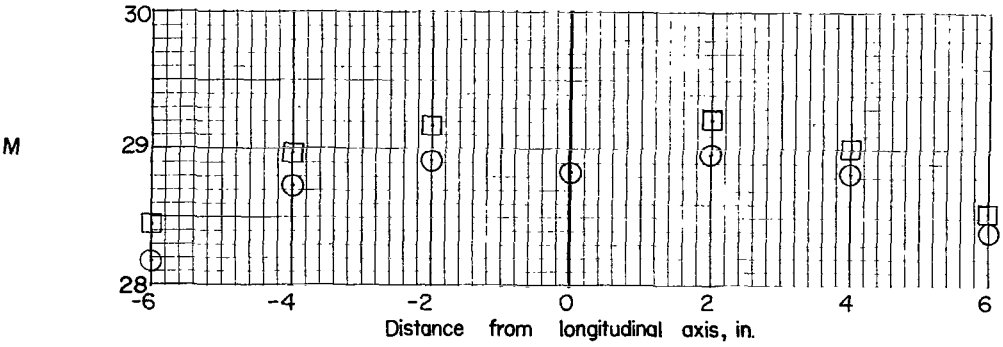

(c) 166.82 inches from throat.

Figure 4.- Mach number calibration of test region for P_t = 2,015 lb/sq in.

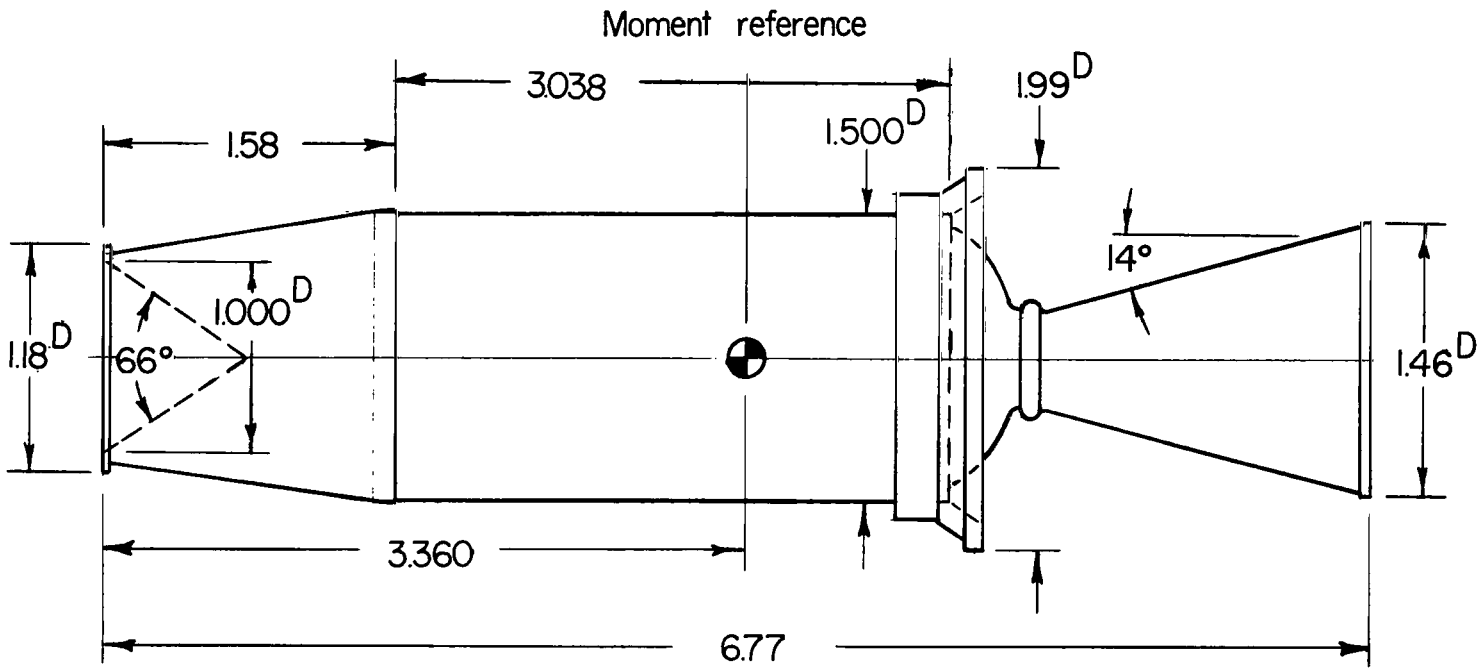

Figure 5.- Detailed model drawing. All dimensions in inches.

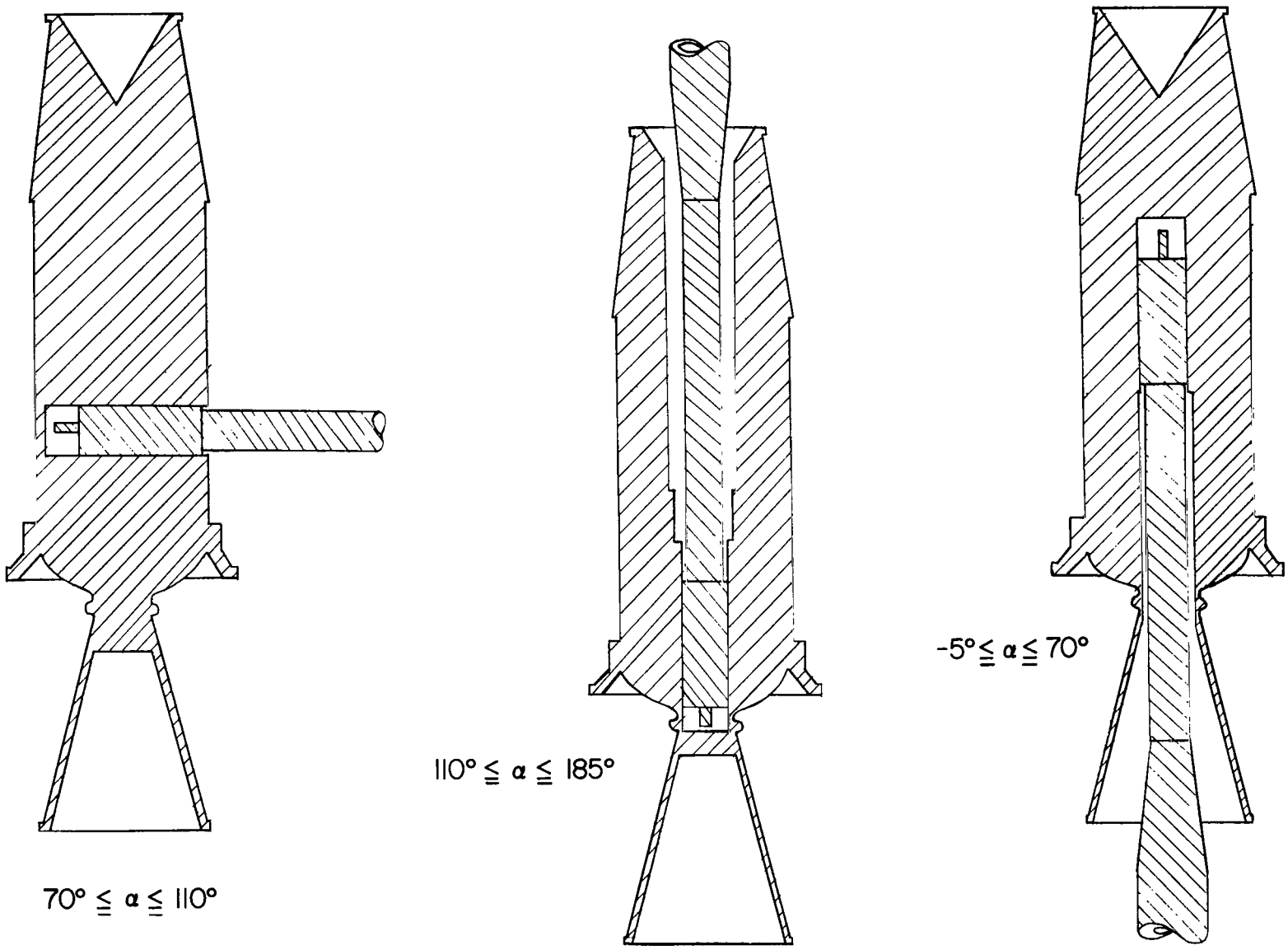

Figure 6.- Model-balance arrangements used to obtain $0^\circ \leqq \alpha \leqq 180^\circ$.

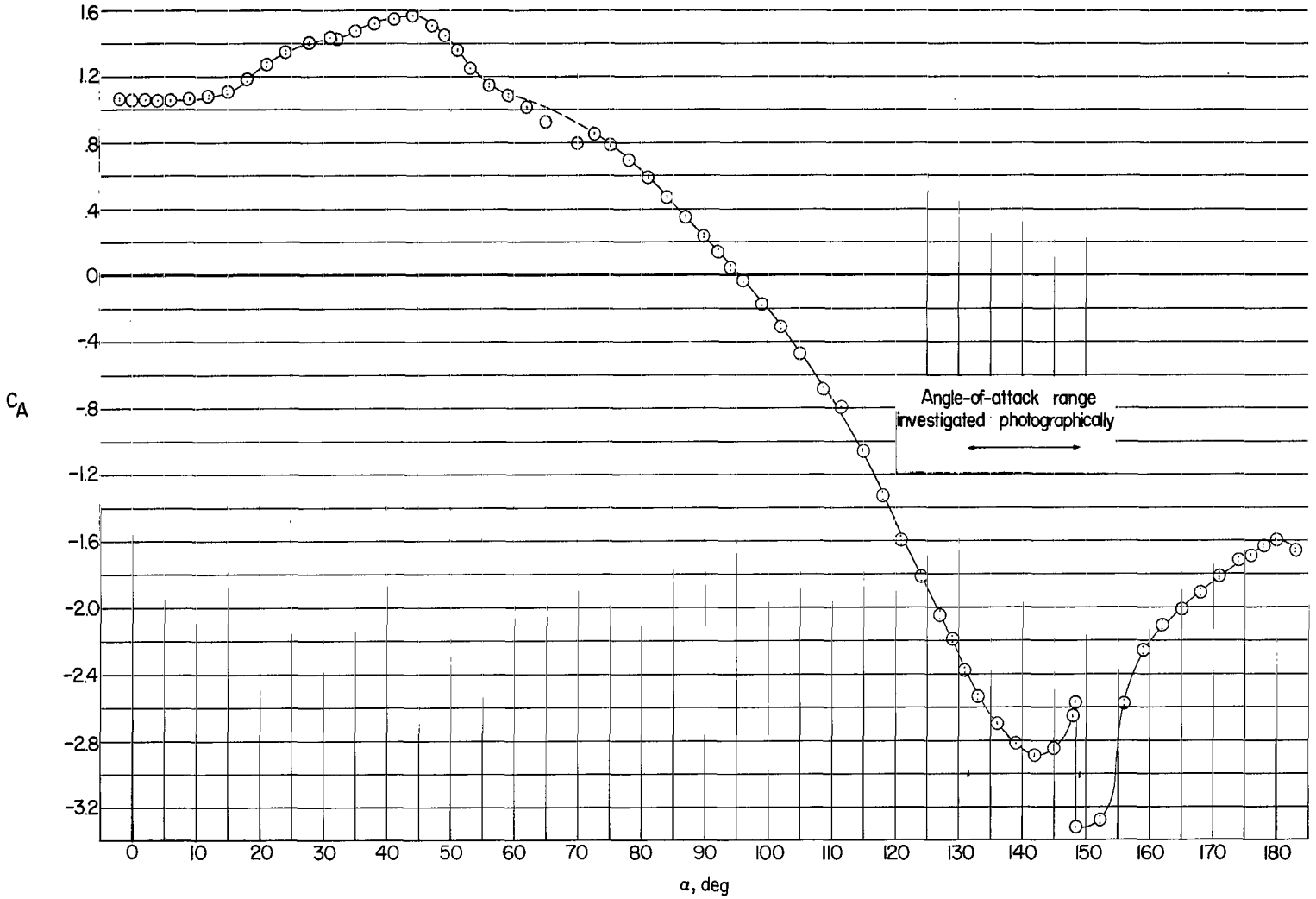

Figure 7.- Variation of axial-force coefficient with angle of attack.

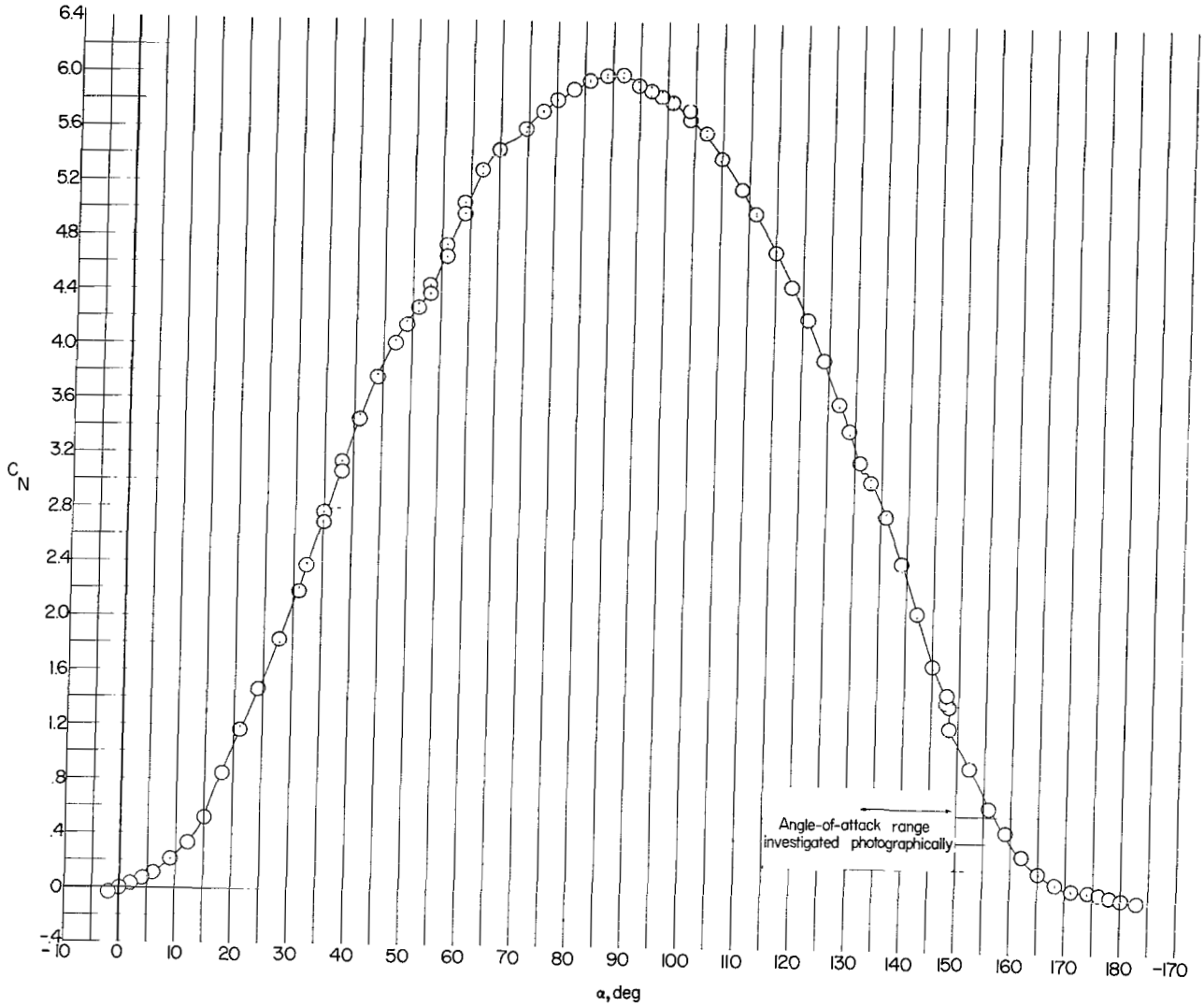

Figure 8.- Variation of normal-force coefficient with angle of attack.

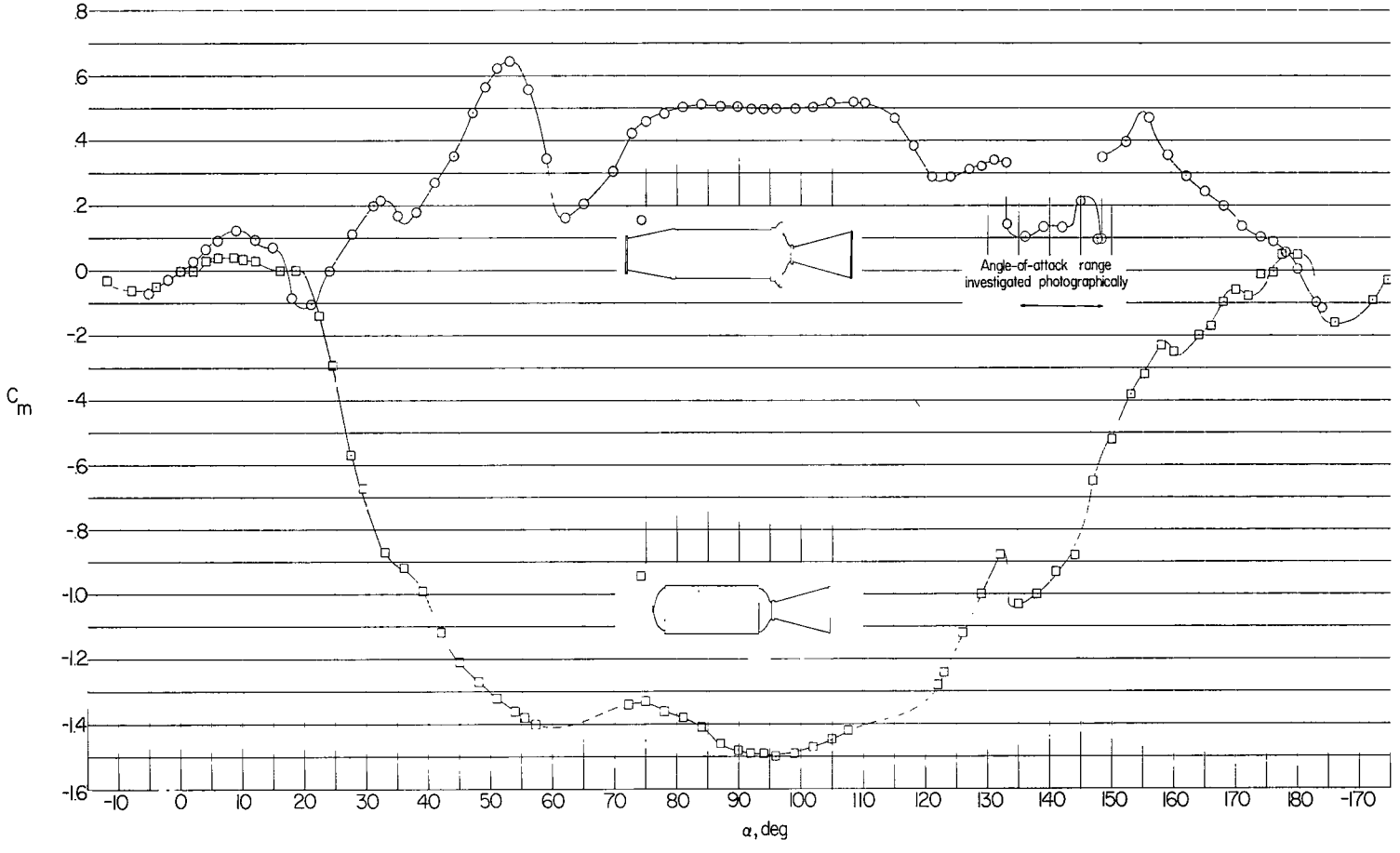

Figure 9.- Variation of pitching-moment coefficient with angle of attack.

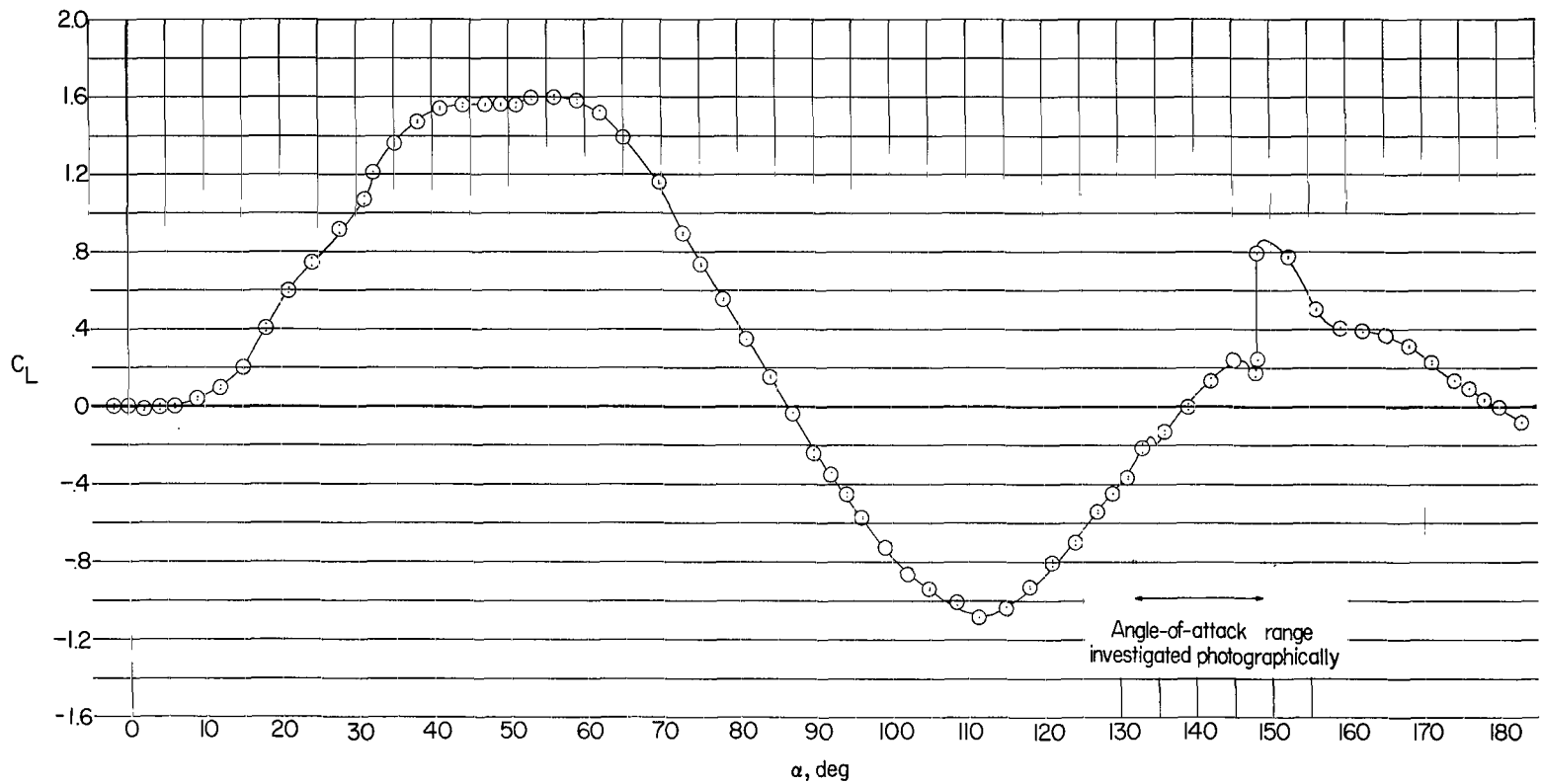

Figure 10.- Variation of lift coefficient with angle of attack.

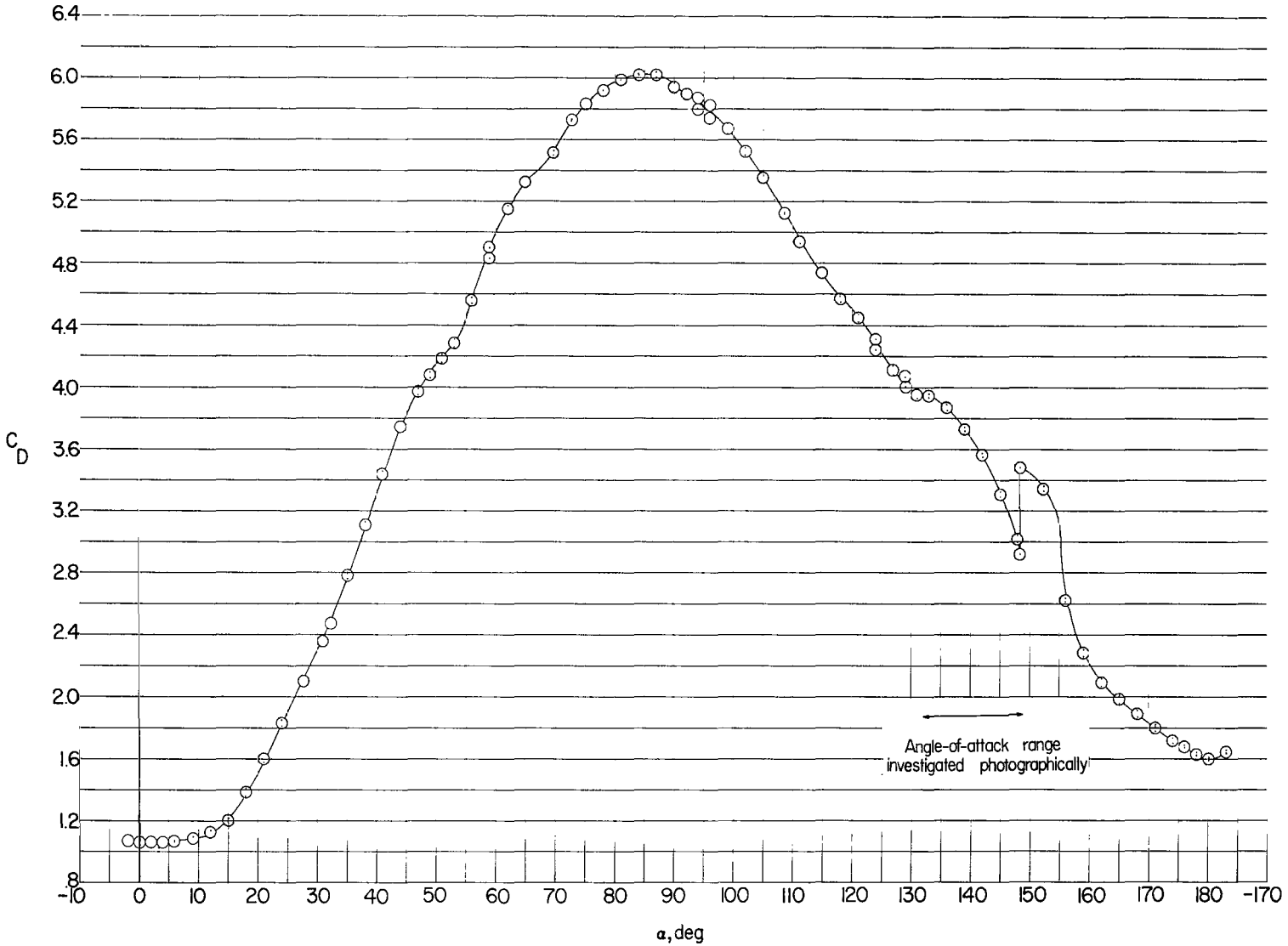

Figure 11.- Variation of drag coefficient with angle of attack.

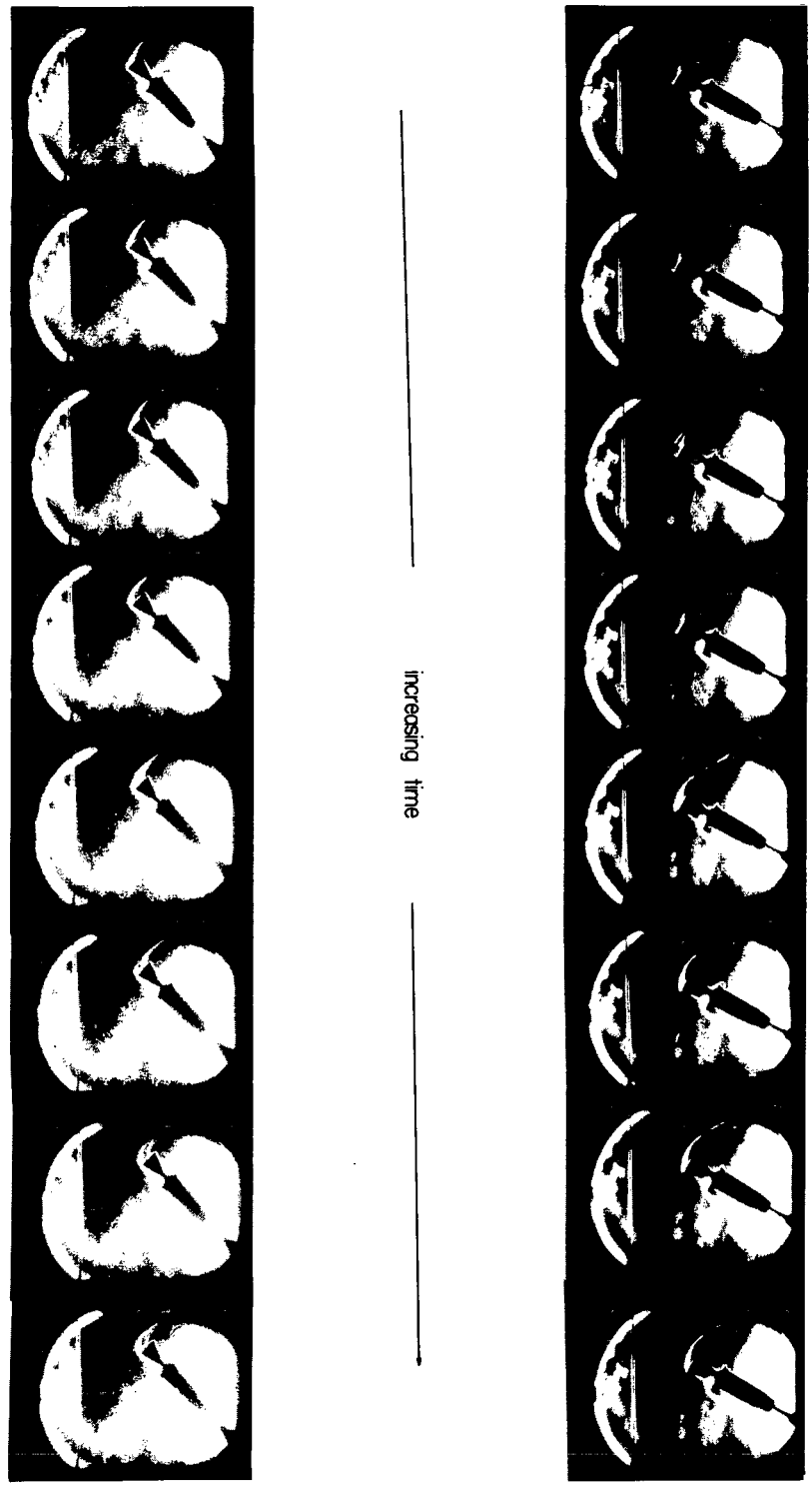

(a) $\alpha \approx 133^{\circ}$.

(b) $\alpha \approx 148^{\circ}$.

L-63-7513

Figure 12.- High-speed photographs of model at specific attitudes (α increasing with time, counterclockwise).

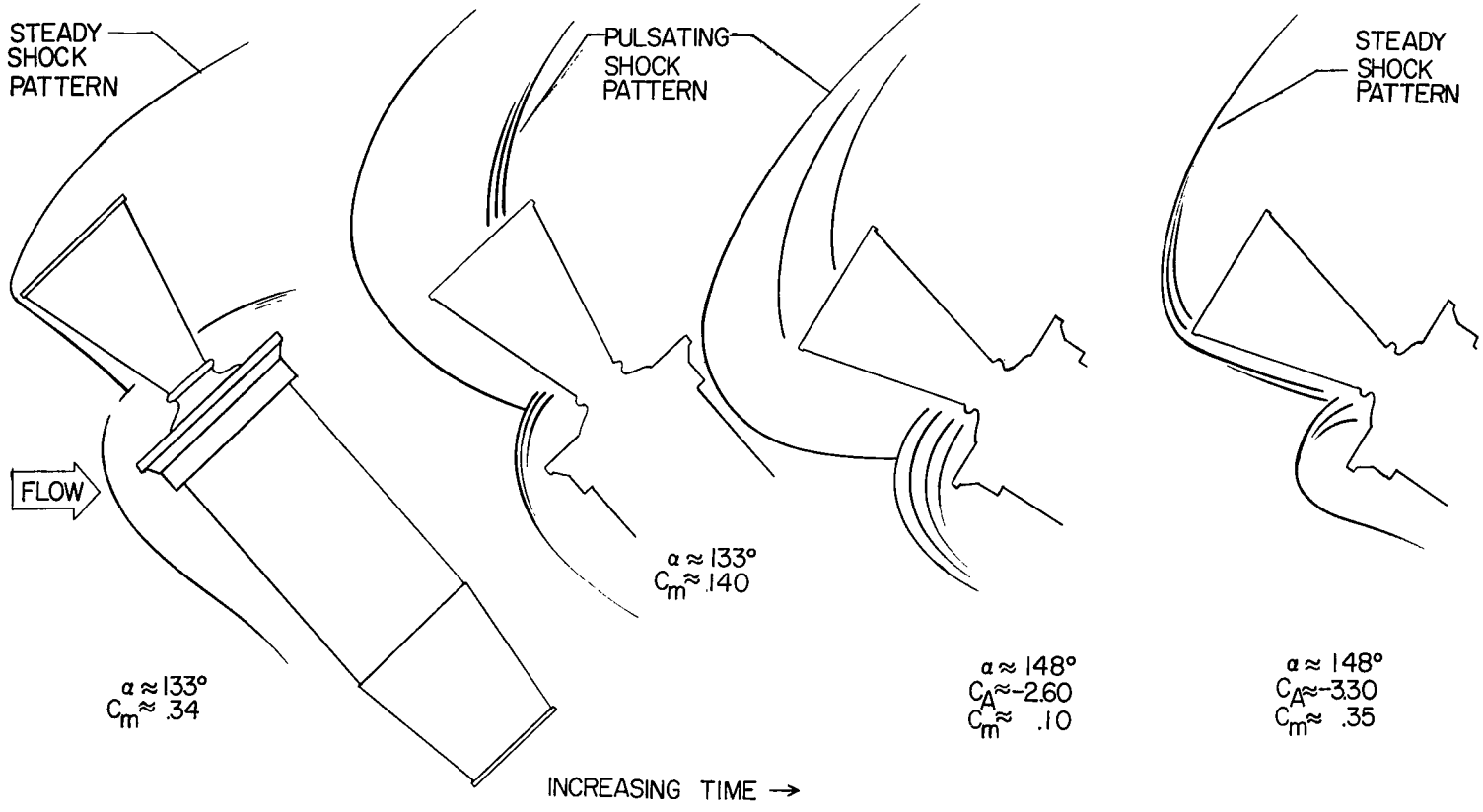

Figure 13.- Sketch of flow phenomena.

NASA-Langley, 1964 L-3612